Detection and discimination of aquacultural facilities in Matsuhima Bay, Japan, for integrated coastal zone management and marine spatial plannning using full polarimetric L-band airborne synthetic aperture radar\n

doi: 10.1080/01431161.2019.1579380

INTERNATIONAL JOURNAL OF REMOTE SENSING
https://doi.org/10.1080/01431161.2019.1579380

Detection and discrimination of aquacultural facilities in Matsushima Bay, Japan, for integrated coastal zone management and marine spatial planning using full polarimetric L-band airborne synthetic aperture radar

Hiroki Murata[a,b,c], Teruhisa Komatsu[b,d] and Chinatsu Yonezawa[c]

[a]Port and Harbor Bureau, City of Yokohama, Yokohama, Japan; [b]Atmosphere and Ocean Research Institute, The University of Tokyo, Kashiwa, Japan; [c]Graduate School of Agriculture Science, Tohoku University, Sendai, Japan; [d]Department of Commerce, Yokohama College of Commerce, Yokohama, Japan

ABSTRACT

Integrated coastal zone management (ICZM) and marine spatial planning (MSP) have been proposed for sustainable development of coastal zones. To implement ICZM and MSP, there is a need to establish database and informational networks to collect, share and disseminate information of the present situation of coastal zones. One permanent and concentrated use of coastal zones is hosting aquacultural facilities. This study aimed to develop a method to detect and discriminate aquacultural facilities in Matsushima Bay, Japan, using L-band polarimetric and interferometric airborne synthetic aperture radar (Pi-SAR-L2). Three-component-scattering model and eigenvalue–eigenvector decomposition were applied. The volume-scattering component images of the three-component-scattering model showed raft, longline, and rack aquacultural facilities from the sea surface in good contrast. The double-bounce-scattering component percentage discriminated rack aquacultural facilities from raft and longline aquacultural facilities. The size difference in the raft and longline aquacultural facilities was helpful for discriminating the type.

ARTICLE HISTORY
Received 31 March 2018
Accepted 16 November 2018

1. Introduction

Coastal zones form an extremely important area supporting not only human activities like shipping, industry, and tourism but also marine food supplies of coastal ecosystems, providing ecosystem services to society. The population of coastal zones has been rapidly increasing, and the food supplied by fisheries is increasingly important. However, world food fish production from capture fisheries is stagnating (World Bank 2013). In contrast, aquacultural products are rapidly increasing and account for nearly one-half of the fish consumed worldwide (FAO 2016). However, aquaculture sometimes affects and changes the coastal environment (e.g. Delgado et al. 1999; Forrest et al. 2009). For sustainable development of coastal zones, integrated coastal zone management (ICZM) was proposed

CONTACT Hiroki Murata murata.ykhm@gmail.com Port and Harbor Bureau, City of Yokohama, Yokohama, Japan

*Present address: Port and Harbor Bureau, City of Yokohama, 2 Yamashita-cho Naka-ku, Yokohama 231-0023, Japan

in Agenda 21 (UNCED 1992). In Japan, the government began enforcing the Basic Act on Ocean Policy in 2007 and is working on ICZM. Recently, marine spatial planning (MSP) has been proposed to improve decision making and deliver an ecosystem-based approach to manage human activities in the marine environment (Ehler and Douvere 2007). This approach uses maps to visualise a more comprehensive picture of the use of a marine area and what natural resources and habitat occur (Baker and Harris 2012). To implement ICZM and MSP, there is a need to establish database and informational networks to collect, share, and disseminate information about the present scenario (Komatsu et al. 2012). In Japan, aquaculture is based on the demarcated fishery right. The area, term, and type of aquaculture are defined by the demarcated fishery rights by the prefecture governors or a minister. The fisheries cooperatives autonomously manage the number and location of aquacultural facilities in a demarcated fishery area on behalf of the prefecture governor or minister. A fisheries cooperative approximately knows these areas but they do not know the exact locations and aquacultural facility types because it is difficult to gather information on numerous aquaculture facilities from field surveys. Governors or ministers do not know their distribution as well. Thus, mapping of aquacultural facilities by type in an efficient manner in a demarcated fishery area to manage it for sustainable use of coastal zones is needed.

Remote sensing can be used to support the planning and management of aquacultural practices and the implementation of adequate regulations and protection measures (Ottinger, Clauss, and Kuenzer 2016). Several studies have attempted to detect aquacultural facilities using optical remote sensing and synthetic aperture radar (SAR) remote-sensing imagery. Optical remote sensing detects the visible, near-infrared, and shortwave infrared radiation of sunlight that reflects from the ground. Komatsu et al. (2002) applied a pan-sharpened IKONOS satellite image of 1 m spatial resolution to detect aquacultural facilities in Yamada Bay, Japan. As a result, 4 m × 12 m raft aquacultural facilities (hereafter referred to as 'RAFT') and 50–100 m longline aquacultural facilities (hereafter referred to as 'LONGLINE') were detected. They also applied 2.5 m spatial resolution pan-sharpened Advanced Land Observing Satellite (ALOS) satellite imagery of Yamada Bay and detected RAFTs and LONGLINEs in most areas except where buoys were less than 1 m below the resolution of the ALOS sensor and where LONGLINEs were submerged under the sea (Komatsu et al. 2012). From these results, it was suggested that high-resolution optical satellite imagery can detect these small-size aquacultural facilities.

SAR actively irradiates and receives microwaves and can observe under all weather conditions, day and night. Hence, SAR can observe more frequently compared to optical satellite imagery. Several studies have detected aquacultural facilities using single polarisation SAR data (e.g. Travaglia et al. 2004; Szuster, Steckler, and Kullavanijaya 2008). During recent years, it has become possible to obtain full polarisation data from air- and space-borne SAR systems. Full polarimetric SAR data provide a scattering matrix of observational objects. The scattering matrix consists of the amplitude and phase at four polarisations, HH, HV, VH, and VV, which are horizontally (H) and vertically (V) polarised waves sent and received by radar antenna. Some polarimetric decomposition methods have been suggested to obtain Earth surface conditions from full polarimetric SAR data. The three-component-scattering model was presented by Freeman and Durden (1998). The four-component-scattering approach was presented by Yamaguchi et al. (2005), and the eigenvalue–eigenvector decomposition was presented by Cloude and Pottier (1996

1997). In a previous study using full polarisation SAR data, Won, Ouchi, and Yang (2013) successfully detected cultivation nets of a size of 123.0 m × 8.3 m in Tokyo Bay, Japan, using the entropy image applied constant false alarm rate (CFAR) based on the eigenvalue decomposition of the ALOS PALSAR data. Sugimoto, Ouchi, and Nakamura (2013) also detected cultivation nets in Tokyo Bay, Japan, by applying four-component-scattering decomposition to ALOS PALSAR data. Although polarimetric SAR has the potential of distinguishing targets according to differences in scattering characteristics, there have been no reports on the classification of types of aquacultural facilities.

In this study, we investigated the possibility of recognising aquacultural facility types by applying the polarimetric decomposition technique to L-band polarimetric and interferometric airborne synthetic aperture radar (Pi-SAR-L2). Pi-SAR-L2 has been operated by the Japan Aerospace Exploration Agency (JAXA) since 2012, and it is possible to obtain imagery with a 1.76 m slant range resolution.

2. Study area and data

2.1. *Study area*

The study area was Matsushima Bay, Sanriku coast, Japan. A wide variety of marine products, such as oyster, scallops, sea pineapple, seaweed, and Coho salmon, are cultured along this coast. Matsushima Bay is at the southern end of the Sanriku coast, and the main cultivation product is oyster. Matsushima Bay is an enclosed bay with an area of approximately 35.3 km^2, a maximum depth of approximately 4 m, and a bay mouth width of approximately 1.7 km (International EMECS Center 2001). Figure 1 shows the distribution of the demarcated fishery right areas and the locations of wave height, weather, and wind observational stations. Three types of oyster aquacultural facilities, (1) RAFT, (2) LONGLINE, and (3) rack (hereafter referred to as 'RACK') facilities, are placed within these demarcated fishery right areas (Figure 2). The size of the RAFT is approximately 5 m × 15 m, the LONGLINE approximately 1 m × 60 m, and the RACK approximately 2–5 m × 60 m. The RAFT is constructed from bamboo poles and buoys. The bamboo poles are fixed in vertical and horizontal directions and to complete a square. After these are combined with buoys, the facility is anchored to the sea bottom. Oysters are hung from the bamboo. The LONGLINE is constructed from buoys and ropes. Both ends of the buoys are bound with ropes to form a single line. Oysters are hung from the rope. This type of facility is mainly placed at the mouth of the bay, where wind and waves are strong. The RACK is placed in the shallow water area. Bamboo poles are pounded into the sea bottom in a parallel arrangement and a crosspiece is set to create the rack. Oysters are hung from the rack.

Matsushima Bay was damaged by the huge tsunami of 11 March 2011. The tsunami destroyed nearly all of the aquacultural facilities (Tsujimoto et al. 2016). Since the occurrence of the tsunami, aquacultural facilities have been recovering year-by-year. We collected field data on the locations and types of aquacultural facilities using a digital camera with Global Positioning System (GPS) tracking on 2 June 2015.

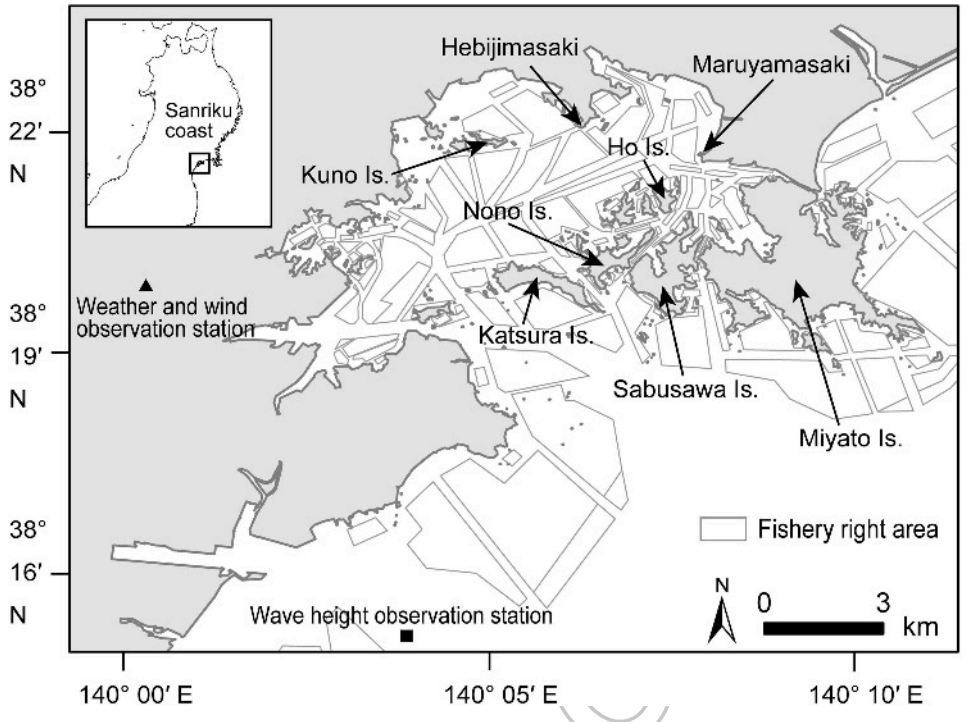

Figure 1. Map of Matsushima Bay with the locations of the demarcated fishery right areas and wave height and weather and wind observational stations.

2.2. *Optical satellite image and aerial photographs*

WorldView-2 data obtained on 28 January 2013 were used as a reference image. WorldView-2 provides a 2.4 m resolution multispectral image in a 20° off-nadir observational mode. At the time of data acquisition, the weather condition was fair. The significant wave height was 0.34 m and the wind speed was 3.5 m s^{-1} from the northwest. The wave height data, acquired at a station approximately 8 km south-southwest of the mouth of Matsushima Bay, were provided by the Nationwide Ocean Wave Information Network for Ports and Harbours (NOWPHAS). The weather and wind data were provided by the Japan Meteorological Agency from a station approximately 3 km west of the inner part of Matsushima Bay (Figure 1). The wind and wave conditions of the study site during the observation were approximately estimated from data obtained from these observational stations. We also referenced aerial photographs acquired on 9 September 2013 and 2 July 2015 by the Geospatial Information Authority of Japan.

2.3. *Pi-SAR-L2 data*

The Pi-SAR-L2 observed Matsushima Bay on 6 August 2014. The altitude, velocity, and pulse repetition frequency were 13,303 m, 230.9 m s^{-1}, and 585.5 Hz, respectively. The pixel size was 1.76 m (illumination) and 3.2 m (airplane flight path). The illumination angle was 10° to 62°. The airplane flew south-southwest to north-northeast and

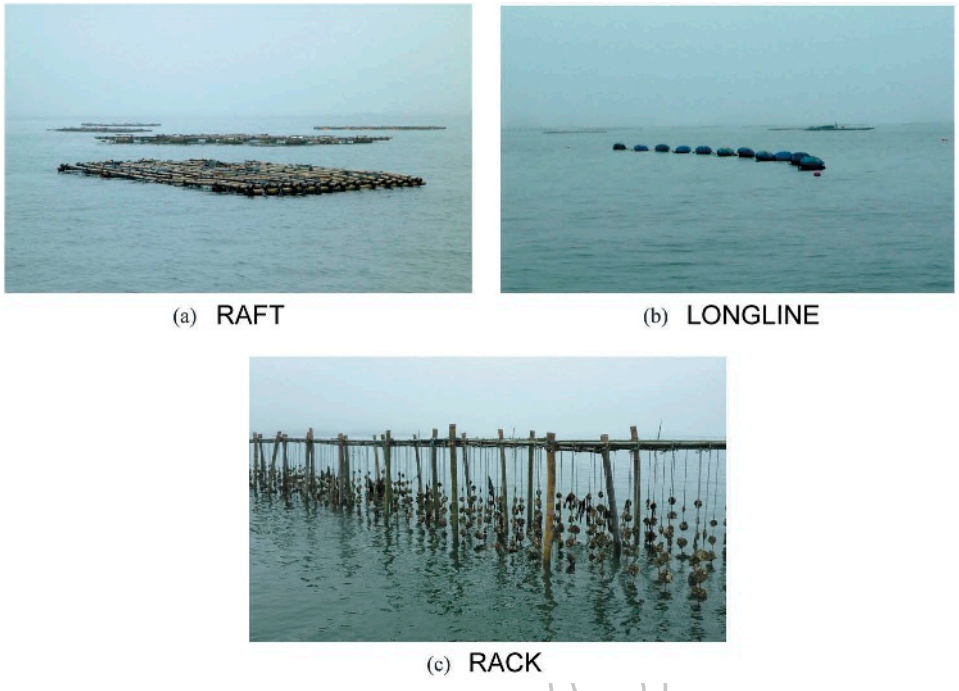

COLOUR FIGURE

Figure 2. Photographs taken on 2 June 2015 of the (a) RAFT, (b) LONGLINE, and (c) RACK oyster aquacultural facility types in Matsushima Bay.

microwave illuminated from the left side. The data were calibrated by JAXA before being made available (Shimada et al. 2013). At the time of data acquisition, the weather condition was fair or cloudy. The significant wave height was 0.62 m, and the wind speed was 3.2 m s^{-1} from the south-southeast.

The Pi-SAR-L2 data were analysed using PolSARpro software. We applied the three-component-scattering model (Freeman and Durden 1998) and eigenvalue–eigenvector decomposition (Cloude and Pottier 1997) using a 3 × 3 pixel window.

The three-component-scattering model decomposes the full polarimetric SAR data into surface, volume, and double-bounce scattering. According to the Freeman and Durden (1998) three-component-scattering model, the total backscatter is as follows:

$$\mathbf{S} = \begin{bmatrix} S_{HH} & S_{HV} \\ S_{VH} & S_{VV} \end{bmatrix} \tag{1}$$

$$\left\langle |S_{HH}|^2 \right\rangle = f_s|\beta|^2 + f_d|\alpha|^2 + f_v \tag{2}$$

$$\left\langle |S_{VV}|^2 \right\rangle = f_s + f_d + f_v \tag{3}$$

$$\left\langle S_{HH}S_{VV}^* \right\rangle = f_s\beta + f_d\alpha + f_v/3 \tag{4}$$

$$\left\langle |S_{HV}|^2 \right\rangle = f_v/3 \tag{5}$$

$$\left\langle S_{HH} S_{HV}^* \right\rangle = \left\langle S_{HV} S_{VV}^* \right\rangle = 0 \tag{6}$$

Here, **S** is the 2 × 2 complex scattering matrix; and f_s, f_d, and f_v are the surface, double-bounce, and volume scatter contributions to the VV polarisation component, respectively. In equations, * means the complex conjugate. Determining whether double-bounce or surface scattering is the dominant contribution by using the sign of $\mathrm{Re}\left(S_{HV} S_{VV}^*\right)$ (Van 1989) enables one to identify the contribution of each scattering mechanism. The parameters α and β are related to double-bounce and surface scatter contributions. Finally, the contribution of each scattering mechanism to the span P were estimated using the following Equations (7) through (10):

$$P = P_s + P_d + P_v = |S_{HH}|^2 + 2|S_{HV}|^2 + |S_{VV}|^2 \tag{7}$$

$$P_s = f_s\left(1 + |\beta|^2\right) \tag{8}$$

$$P_d = f_d\left(1 + |\alpha|^2\right) \tag{9}$$

$$P_v = 8 f_v/3 \tag{10}$$

We calculated the percentage of surface, double-bounce, and volume scattering in the total backscatter.

Polarimetric parameters, entropy (H), and alpha angle ($\bar{\alpha}$) were computed using eigenvalue–eigenvector decomposition. According to Cloude and Pottier (1997), the coherency matrix is defined by the following equation:

$$\begin{aligned} T &= \frac{1}{2}\left\langle \begin{bmatrix} (S_{HH}+S_{VV})(S_{HH}+S_{VV})^* & (S_{HH}+S_{VV})(S_{HH}-S_{VV})^* & 2(S_{HH}+S_{VV})S_{HV}^* \\ (S_{HH}-S_{VV})(S_{HH}+S_{VV})^* & (S_{HH}-S_{VV})(S_{HH}-S_{VV})^* & 2(S_{HH}-S_{VV})S_{HV}^* \\ 2S_{HV}(S_{HH}+S_{VV})^* & 2S_{HV}(S_{HH}-S_{VV})^* & 4S_{HV}S_{HV}^* \end{bmatrix} \right\rangle \\ &= \mathbf{U}_3 \begin{bmatrix} \lambda_1 & 0 & 0 \\ 0 & \lambda_2 & 0 \\ 0 & 0 & \lambda_3 \end{bmatrix} \mathbf{U}_3^{*T} \end{aligned} \tag{11}$$

where the parameters λ_1, λ_2, and λ_3 are the calculated eigenvalues of **T**, conventionally ordered such that $0 \le \lambda_3 \le \lambda_2 \le \lambda_1$. Matrix $\mathbf{U}_3$ is parameterised as follows:

$$\mathbf{U}_3 = \begin{bmatrix} \cos\alpha_1 & \cos\alpha_2 & \cos\alpha_3 \\ \sin\alpha_1 \cos\beta_1 e^{i\delta_1} & \sin\alpha_2 \cos\beta_2 e^{i\delta_2} & \sin\alpha_3 \cos\beta_3 e^{i\delta_3} \\ \sin\alpha_1 \sin\beta_1 e^{i\gamma_1} & \sin\alpha_2 \sin\beta_2 e^{i\gamma_2} & \sin\alpha_3 \sin\beta_3 e^{i\gamma_3} \end{bmatrix} \tag{12}$$

Parameter α_i is directly related to the angle of incidence and dielectric constant of the surface with i ranging from 1 to 3. The β_i angles can be interpreted as orientation angles. γ_i and δ_i account for the phase relations. The appearance probability of each λ_i contribution is given by the following:

$$P_i = \frac{\lambda_i}{\sum_{j=1}^{n} \lambda_j} \tag{13}$$

The polarimetric scattering entropy is defined as follows:

$$H = \Sigma_{i=1}^{n} - P_i \log_n P_i (0 \le H \le 1) \tag{14}$$

where $n = 3$ for backscatter problems. The randomness of the scattering process is measured by the entropy. The dominant scattering mechanism for each pixel is provided by the alphaangle($\overline{\alpha}$):

$$\overline{\alpha} = P_1\alpha_1 + P_2\alpha_2 + P_3\alpha_3 (0° \le \overline{\alpha} \le 90°) \tag{15}$$

3. Results and discussion

3.1. *Estimation of the aquacultural facility distribution using an optical image*

Estimated distributions of the three aquacultural facility types in Matsushima Bay were mapped from a WorldView-2 image on 28 January 2013 using visual interpretation (Figure 3). The aerial photograph obtained during September 2013 supported the interpretation. The RAFTs were mainly to the north of Katsura Island and to the west of Miyato Island. The LONGLINEs were mainly north-northeast of Katsura Island, north-northwest of Nono Island, and north-northwest and east of the Ho Islands. The RACKs

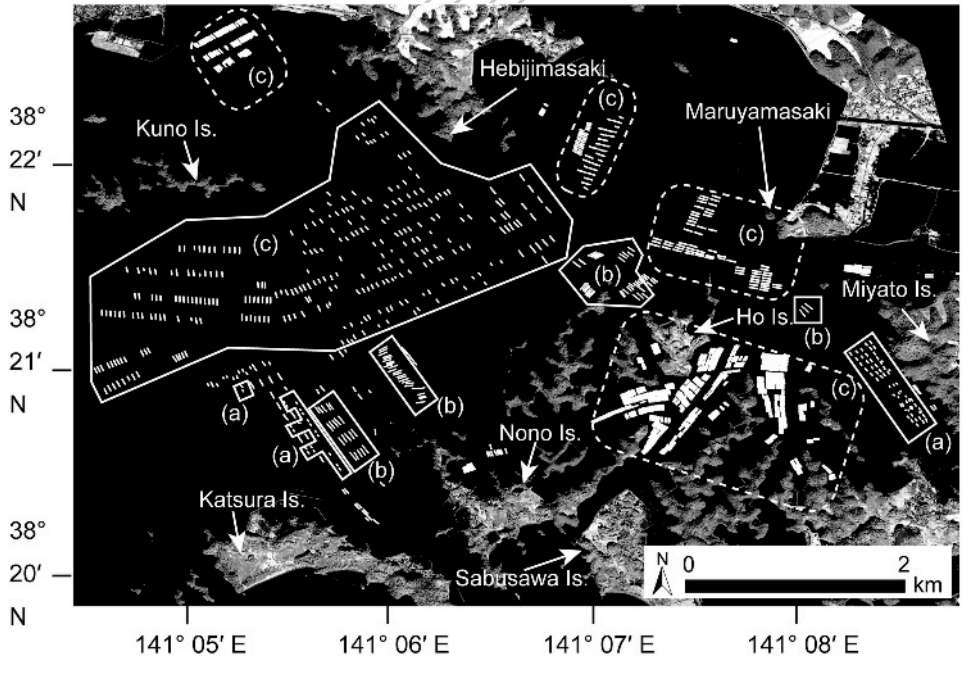

Figure 3. Estimated distributions of the (a) RAFT, (b) LONGLINE, and (c) RACK aquacultural facilities in Matsushima Bay on 28 January 2013 from a WorldView-2 image with a near-infrared image. Densely located RACKs are shown in dashed rounded rectangular outlines and others are shown in solid rectangular outlines and polygons.

were extensively distributed in the bay. The RACKs were distributed at a relatively low density, except in the area north-northeast of Kuno Island; the area surrounded by the Nono, Sabusawa, and Ho islands; the area east of Hebijimasaki; and the area southwest of Maruyamasaki. In Figure 3, densely distributed RACKs are shown by dashed rounded rectangular outlines and others are shown by solid rectangular outlines and polygons.

3.2. *Detection of an aquacultural facility using HH or HV single polarimetric images of Pi-SAR-L2*

Figure 4 shows an (a) horizontal-horizontal (HH) single polarisation image and an (b) horizontal-vertical (HV) single polarisation image of Pi-SAR-L2 data for 6 August 2014. The black colour indicates small scattering, and the white colour large scattering. The HH single polarisation image indicated a different scale of colour on sea surface by area (Figure 4(a)). The northern area of Nono island; the area surrounded by the Nono, Sabusawa, and Ho islands; and the western area of Maruyamasaki and Hebijimasaki showed small scattering from the sea surface. At the time of data acquisition, the wind direction was from south-southeast. Therefore, it is considered that the islands blocked the wind and affected the sea surface roughness. At these areas, aquacultural facilities showed good contrast with the sea surface compared to that of other areas and could be detected. However, it was difficult to clearly detect aquacultural facilities in the study area except for these areas. The HV single polarisation image showed small scattering from the sea surface and large scattering from the aquacultural facilities (Figure 4(b)). Therefore, from the HV single polarisation image we clearly detected aquacultural facilities from the sea surface of the study area. From this HV single polarisation image, aquacultural facilities that were not recognised from the WorldView-2 image (Figure 3) were detected. These aquacultural facilities are shown in the dashed rectangular outlines and polygon in Figure 4(b). This can be explained by the year-by-year recovery of aquacultural facilities after the tremendous tsunami damage that occurred on 11 March 2011.

The aquacultural facilities were detected using HH or HV single polarisation images. Particularly, the HV single polarisation image showed small scattering from the sea surface and we could detect aquacultural facilities in good contrast compared to the HH single polarisation image. However, the aquacultural facility type was difficult to discriminate only using the HH or HV single polarisation images.

3.3. *Discrimination of aquacultural facility types using polarimetric analysis of Pi-SAR-L2 data*

The three-component decomposition image of Pi-SAR-L2 data for 6 August 2014 is shown in Figure 5. This image indicated double-bounce scattering as red, volume scattering as green, and surface scattering as blue to better differentiate all three scatterings in one figure. To compare each scattering component image of the three-component scattering model and the eigenvalue–eigenvector decomposition, we focused on three the (a) RAFT, (b) LONGLINE, and (c) RACK where each aquacultural facility type was intensively located as shown in Figure 5. The incident angle was approximately 35° for (a) RAFT and 45° for both (b) LONGLINE and (c) RACK. Each

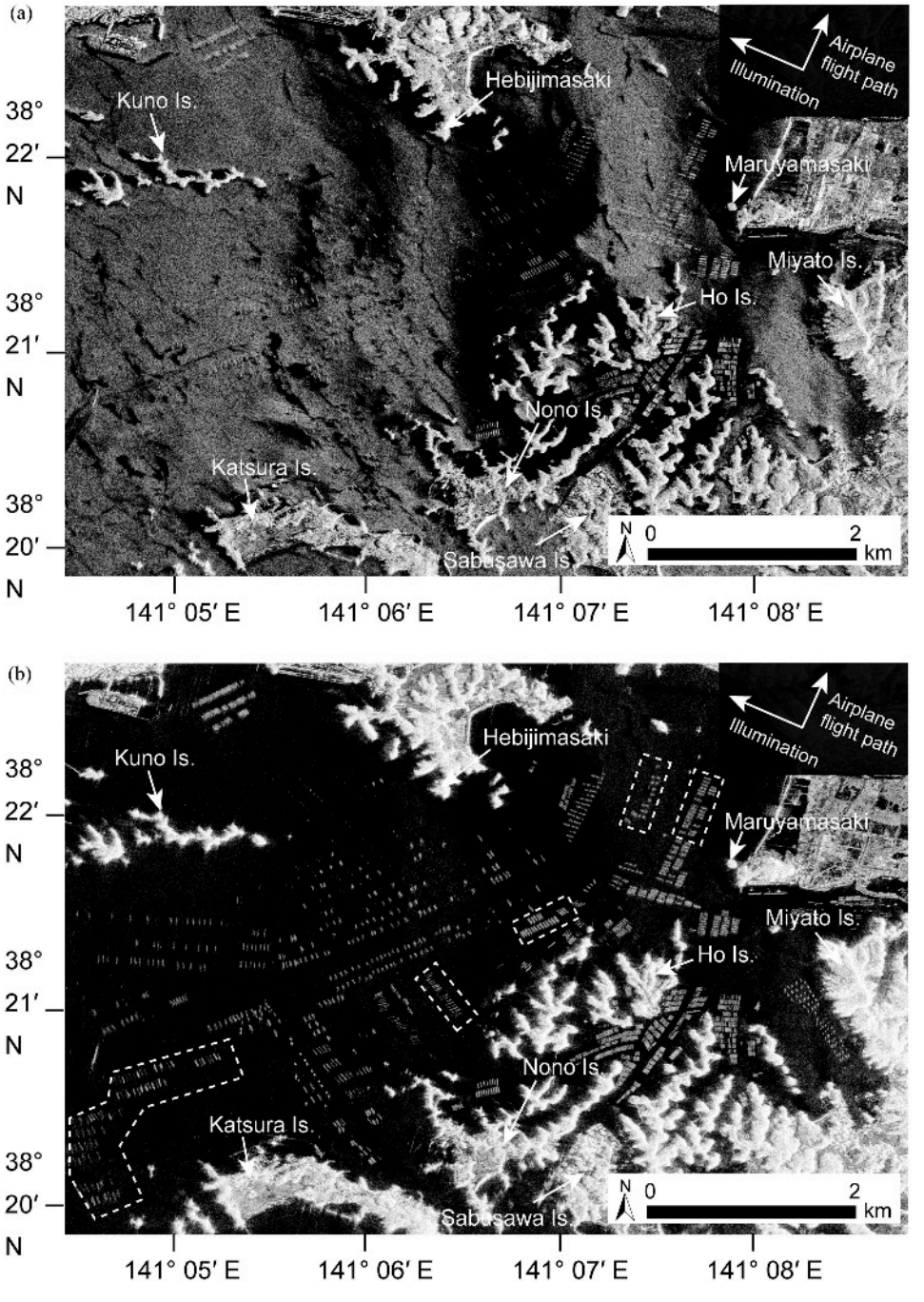

Figure 4. Images show (a) HH single polarisation and (b) HV single polarisation of Pi-SAR-L2 data for 6 August 2014. The black colour shows small scattering and the white colour large scattering. Dashed rectangular outlines and polygons in (b) show the distributions of the aquacultural facilities that were not recognised on the WorldView-2 image from 28 January 2013 (Figure 3).

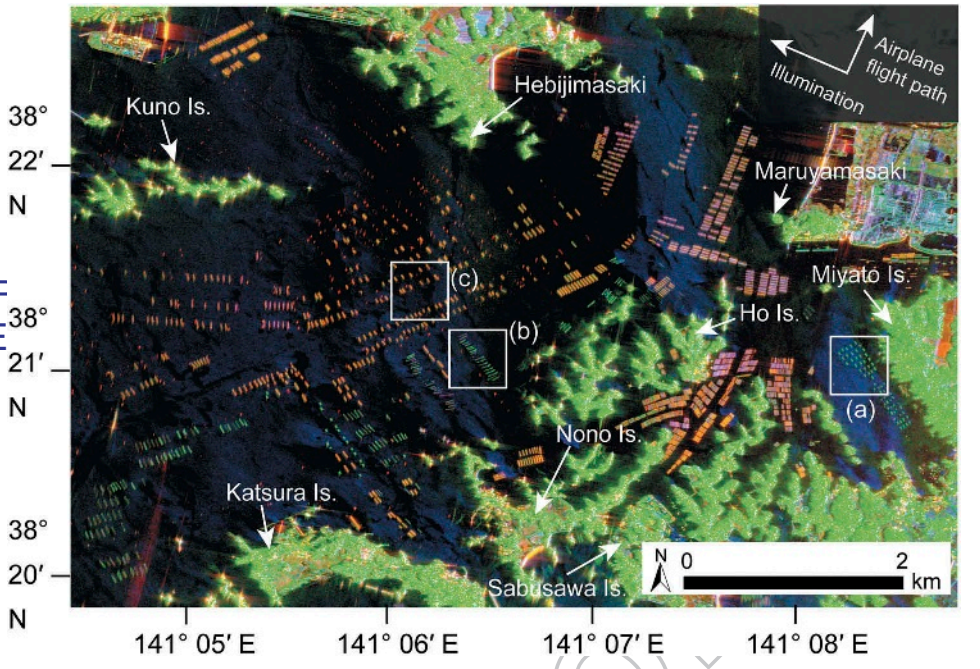

Figure 5. Three-component decomposition image of Pi-SAR-L2 data for 6 August 2014. The image shows double-bounce scattering as red, volume scattering as green, and surface scattering as blue. Solid squares show areas of (a) RAFT, (b) LONGLINE, and (c) RACK aquacultural facilities, focused to compare the scattering component images shown in Figure 6.

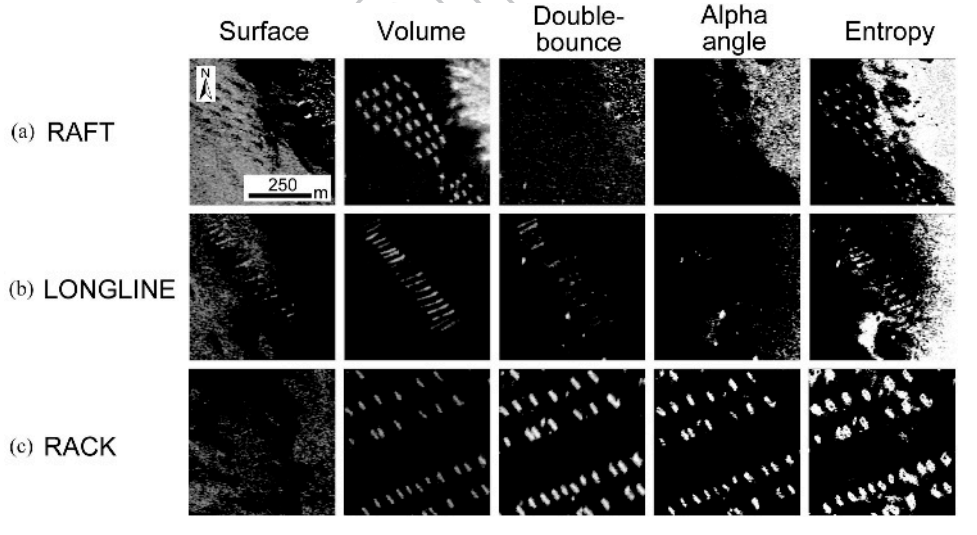

Figure 6. Surface, volume, and double-bounce-scattering images of the three-component-scattering model and alpha angle and entropy images of the eigenvalue–eigenvector decomposition. The black colour shows small scattering and the white colour large scattering. The selected areas of the (a) RAFT, (b) LONGLINE, and (c) RACK types are shown in Figure 5.

scattering component image of three are shown in Figure 6 to compare the detectability. The black colour indicates small scattering and the white colour indicates large scattering. The RAFTs and LONGLINEs were mainly detected using volume scattering, and the RACKs the volume scattering component, double-bounce scattering component, alpha angle, and entropy images. The three aquacultural facility types were commonly clearly detected using volume scattering component images. HV polarisation greatly contributes to the volume scattering component. Therefore, it is considered that HV single polarisation images may be suitable to detect aquacultural facilities that are in good contrast with the sea surface. This result confirms the result in the previous chapter 3.2.

Table 1 shows the average and standard deviation of the surface, volume, and double-bounce scattering computed using the three-component scattering model and the alpha angle and entropy using eigenvalue–eigenvector decomposition. The contributions of the scattering components were individually computed inside the solid rectangular outlines and polygons as (a) RAFT, (b) LONGLINE, and (c) RACK shown in Figure 3. These aquacultural facilities inside the solid rectangular outlines and polygons that had been placed at the time of the WorldView-2 observation on 28 January 2013 were selected for polarimetric analysis. The aquacultural facilities that were not recognised and are not shown in Figure 3, and the aquaculture facility types that had changed between January 2013 and July 2015 as detected in the aerial photograph, were not part of the polarimetric analysis. The number of samples of the aquaculture facilities was 80 for the RAFTs, 72 for the LONGLINEs, and 210 for the RACKs. In addition, 50 sample areas of the sea surface were selected in the study area to compare to the aquacultural facilities.

Figure 7 shows an image of the dominant scattering components of the three aquacultural facility types and sea surface. Volume scattering was dominant and surface scattering was the second most important contribution to the RAFTs. The average of the volume-scattering component percentage was 1.38 times greater than the average of the surface-scattering component percentage. The double-bounce-scattering component percentage of the RAFTs was very small with an average of 0.6%. The inner structure of the RAFTs may cause volume-scattering, and microwaves reflecting from the surface of the RAFTs may cause surface scattering (Figure 7(a)).

Surface scattering was dominant and volume scattering was the second-greatest contributor for the LONGLINEs (Figure 7(b)). The average of the surface-scattering component

Table 1. Average and standard deviation of the surface, volume, and double-bounce scattering values computed using the three-component-scattering model, and the alpha angle and entropy using eigenvalue–eigenvector decomposition. Aquacultural facilities selected inside the solid rectangular outlines and polygons are individually shown in Figure 3.

		RAFT		LONGLINE		RACK		Sea surface	
		Avg	SD	Avg	SD	Avg	SD	Avg	SD
Three–component-scattering model	Surface (%)	41.7	19.3	63.1	20.3	27.1	16.8	90.7	9.3
	Volume (%)	57.7	19.6	33.5	21.6	20.4	8.3	7.4	6.4
	Double-bounce (%)	0.6	1.1	3.4	3.0	52.6	13.8	2.0	3.3
Eigenvalue–eigenvector decomposition	Entropy	0.51	0.10	0.43	0.09	0.63	0.05	0.20	0.15
	Alpha angle (°)	28.55	5.75	25.79	6.02	50.54	7.51	21.99	3.73

Avg*: Average
SD**: Standard deviation

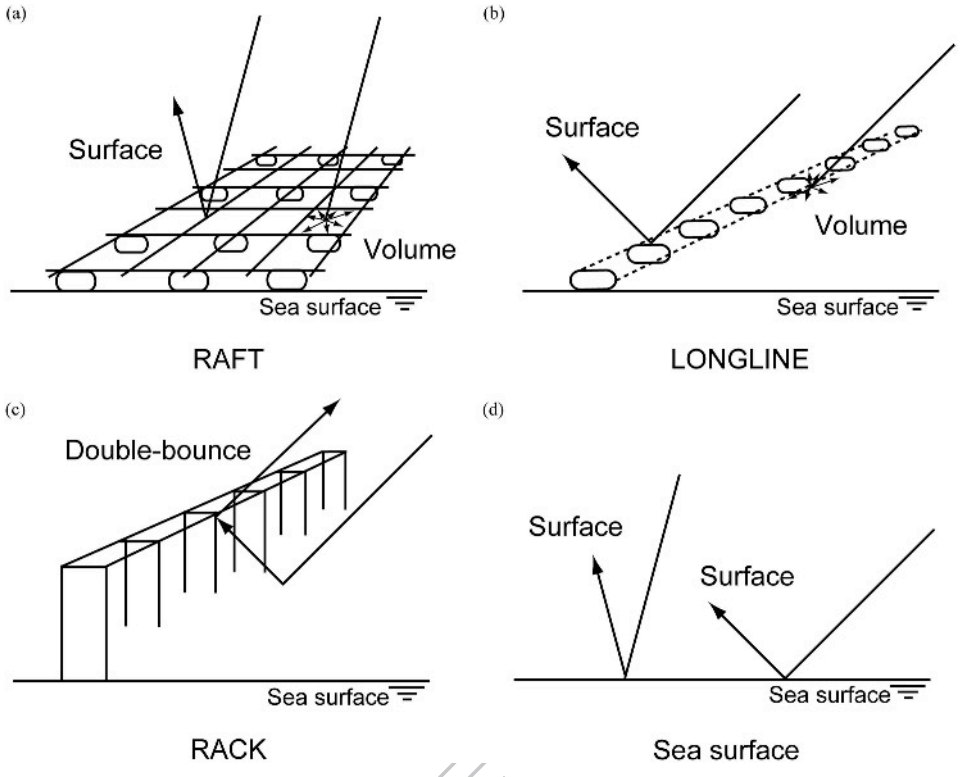

Figure 7. Image of the dominant scattering components of the three aquacultural facility types (a) RAFT, (b) LONGLINE, and (c) RACK as well as the (d) Sea surface.

percentage was 1.88 times greater than the average of the volume-scattering component percentage. The average of the double-bounce-scattering component percentage was 3.4%. This value was small, but greater than that of the RAFTs.

For the RACK, the average of the double-bounce-scattering component percentage accounted for more than one-half of all of the scattering components. The RACKs showed a larger double-bounce-scattering component percentage compared to that of the RAFTs or LONGLINEs. This was likely because the RACKs are constructed from bamboo pounded into the sea bottom and the microwaves were reflected twice, at the sea surface and bamboo (Figure 7(c)). On average, the surface-scattering component accounts for a greater percentage than the volume-scattering component. The incidence angle of the analysed RACK and LONGLINE areas is approximately 45°. This incidence angle caused an obvious difference in the scattering component percentages in the aquacultural facility types in this study.

The sea surface accounted for 90.7% of the average of the surface-scattering component percentage. This percentage was greater than that of the three aquacultural facility types. The average value of the alpha angle was 0.20 which was less than that of the three aquacultural facility types.

Figure 8 shows triangle plots of the surface, volume, and double-bounce-scattering component percentages computed from the three-component-scattering model for three aquacultural facility types and sea surface samples. The selected samples were

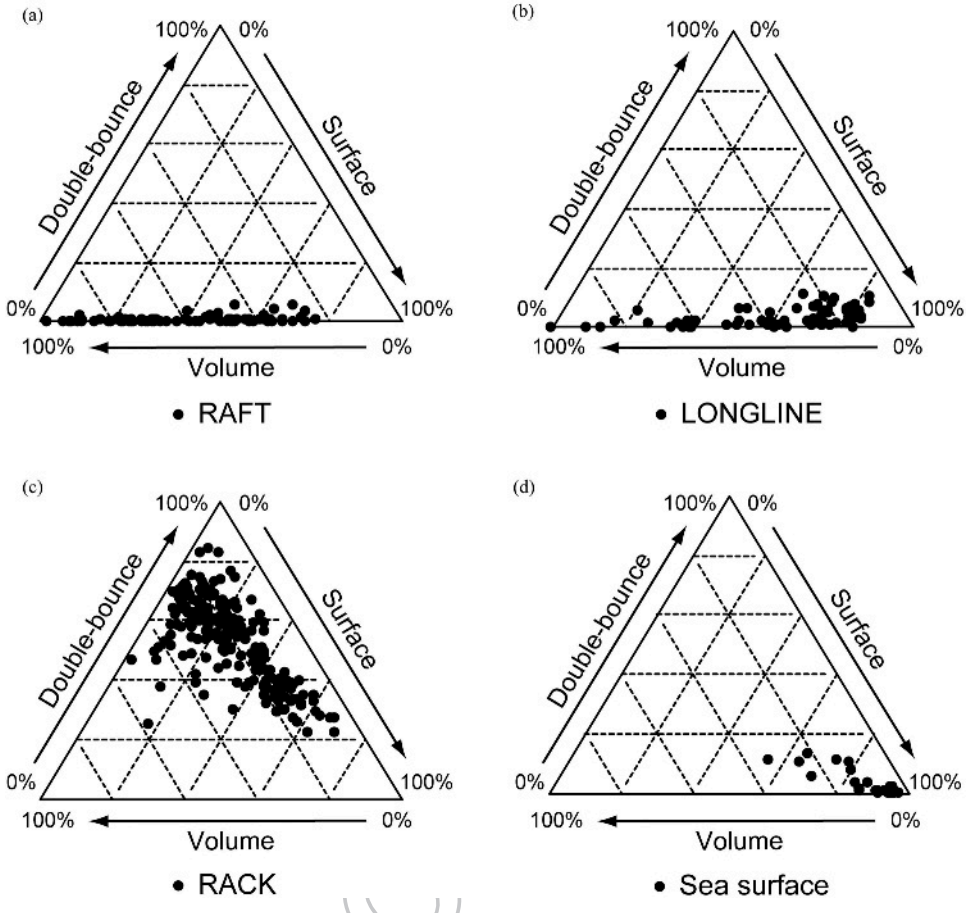

Figure 8. Triangle plots of surface, volume, and double-bounce-scattering component percentages of the three aquacultural facility types and sea surface samples. The aquacultural facility types (a) RAFT, (b) LONGLINE, and (c) RACK were selected inside the solid rectangular outlines and polygons shown in Figure 3 and (d) Sea surface was extensively recorded in the study area.

the same as those selected in Table 1. The RAFTs showed widely ranging surface (2–76%) and volume (24–98%)-scattering component percentages, but the range of the distribution of double-bounce (0–6%)-scattering component percentages was narrower than that of the other two components. The LONGLINEs showed a more widely ranging distribution of surface (0–85%), volume (6–100%), and double-bounce (0–11%)-scattering component percentages than that of the RAFTs. The widespread distribution of the volume-scattering component of the LONGLINEs may be because the LONGLINEs mainly consist of buoys, which scatter microwaves in all directions (Figure 7(b)). Some LONGLINEs showed a small contribution of double-bounce scattering. It is assumed that buoys were drier than the sea surface and that microwaves reflected twice, at the sea surface and at the buoy. Therefore, the double-bounce-scattering component will increase if the buoy is floating and drier than the sea surface. Sugimoto, Ouchi, and Nakamura (2013) concluded that surface scattering showed good contrast for detecting cultivation nets underwater. Thus, if buoys are sinking, it seems likely that the surface-

scattering component percentage would increase and the double-bounce-scattering component percentage would relatively decrease. Therefore, the scattering component percentage is affected by the position relation between the buoy and the sea surface.

The RACKs showed widely ranging surface (2–71%), volume (5–57%), and double-bounce (22–84%) -scattering components. The RACKs showed a larger double-bounce-scattering component percentage range than that of the RAFTs and LONGLINEs. Thus, it should be possible to discriminate the RACKs from RAFTs and LONGLINEs using the contribution of double-bounce scattering. As shown in Figure 8 (c), aquacultural facilities showing a double-bounce-scattering component percentage greater than 20% were assumed to be RACKs. The RAFTs and LONGLINEs showed a similar distribution of scattering component percentages. Thus, it was difficult to discriminate the RAFTs and LONGLINEs from the scattering component percentage of the three-component decomposition model. To discriminate the RAFTs and LONGLINEs, it was helpful to use the size difference of the facilities to estimate the facility type. The length of a RAFT is approximately 15 m, and the length of a LONGLINE or RACK is approximately 60 m. Therefore, the RAFTs can be discriminated from the other two types of facilities using their size difference.

The sea surface showed widely ranging surface (56–97%), volume (3–33%), and double-bounce (0–13%)-scattering component percentages. The double-bounce-scattering component percentage of the sea surface was less than that of the RACKs and was possible to discriminate. The average surface-scattering component was 90.7% and nearly all samples showed a greater than 90% surface scattering as shown in Figure 8 (d). However, some samples showed a smaller percentage. Hence, overlaps existed between the aquacultural facilities and sea surface. This was considered a result of the sea surface roughness being affected by geographical features and weather conditions.

The eigenvalue–eigenvector decomposition results for individual samples are shown in Figure 9. The selected samples were the same as those selected in Table 1. For the RAFTs, the alpha angle distributes between 18° and 43° and the entropy between 0.23 and 0.74. For the LONGLINEs, the alpha angle distributes between 15° and 44° and the entropy between 0.25 and 0.75. The RACKs showed a distribution of alpha angle from 33° to 65° and a distribution of entropy from 0.41 to 0.75. Sea surface showed an alpha angle distribution between 16° and 33° and entropy between 0.08 and 0.66. The RAFTs and LONGLINEs showed approximately the same data ranges for alpha angle and entropy. The RACKs showed a larger alpha angle and entropy value than those of the other two facility types. However, overlaps in the data distributions for both alpha angle and entropy were found between the RACKs and the other two aquacultural facility types. The RACKs showed the same or a larger alpha angle data range compared to that of the sea surface and it should be possible to discriminate nearly all of the RACKs from the sea surface. Other results showed overlaps and it was difficult to discriminate aquacultural facilities from the sea surface using eigenvalue-eigenvector decomposition.

4. Conclusions

Pi-SAR-L2 data were applied to detect and discriminate three aquacultural facility types, RAFTs, LONGLINEs, and RACKs, in Matsushima Bay. Using HH and HV single polarisation images one could detect the aquaculture facilities. Particularly, the HV single polarisation image showed good contrast between the aquacultural facilities and sea surface and

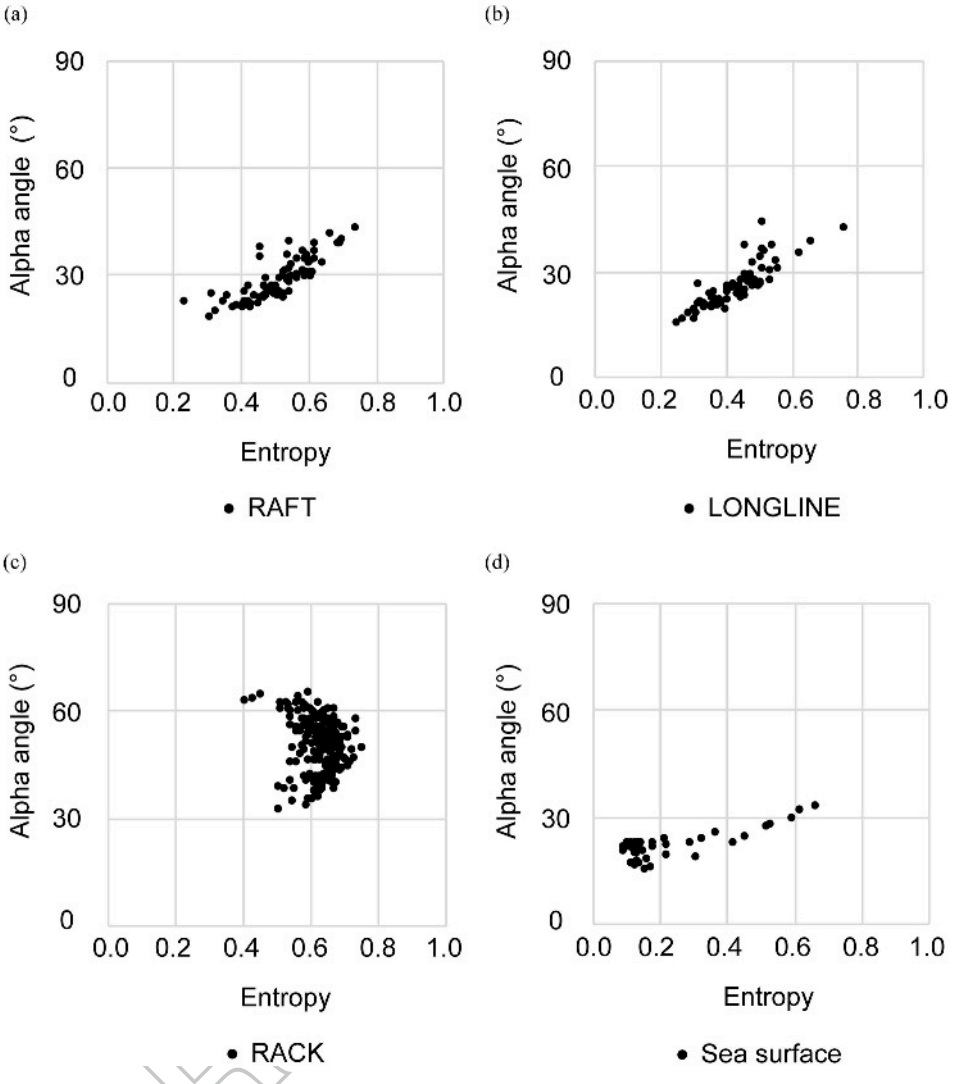

Figure 9. Plots of alpha angle and entropy for the (a) RAFT, (b) LONGLINE, (c) RACK aquacultural facilities and (d) Sea surface. The aquacultural facilities were selected inside the solid rectangular outlines and polygons shown in Figure 3 and (d) Sea surface was selected throughout the study area.

they were clearly detected throughout the study area. However, the aquacultural facility types were difficult to discriminate using only these images.

Polarimetric analysis of the three-component-scattering model discriminated the RACKs from RAFTs and LONGLINEs because of the larger double-bounce-scattering component percentage. The RACKs were also discriminated from the sea surface using their larger double-bounce-scattering component percentage. The RAFTs and LONGLINEs were difficult to discriminate using the scattering component percentages of three-component-scattering model. To discriminate the RAFTs and LONGLINEs, the size difference was helpful in estimating. The result of the alpha angle of the eigenvalue-eigenvector

decomposition could discriminate nearly all of the RACKs from the sea surface. However, the three aquacultural facility types were difficult to discriminate because the data overlapped.

The weather, wave height, and wind speed were considered to be suitable at the Pi-SAR-L2 observed time. If the weather condition is not suitable, detection and discrimination of aquacultural facilities may become difficult. Matsushima Bay is an enclosed bay; therefore, the sea surface in the bay is calm compared to that in other coastal areas. Thus, geographical features are considered important in detecting and discriminating aquacultural facilities.

Acknowledgments

The Pi-SAR-L2 data are copyrighted by the Japan Aerospace Exploration Agency (JAXA). The WorldView-2 data were provided by a portion of the project of the Mitsui & Co. Environment Fund, 2011. This study was supported by Grants-in-Aid by the Tohoku Ecosystem-Associated Marine Sciences (TEAMS) from the Japan Ministry of Education, Culture, supports, Science and Technology, and a Sasakawa Scientific Research Grant from The Japan Science Society.

Disclosure statement

AQ2 No potential conflict of interest was reported by the authors.

References

Baker, E. K., and P. T. Harris. 2012. "Habitat Mapping and Marine Management." In *Seafloor Geomorphology as Benthic Habitat: GeoHab Atlas of Seafloor Geomorphic Features and Benthic*
AQ3 *Habitats*, edited by P. T. Harris and E. K. Baker, 23–38. Amsterdam: Elsevier.

Cloude, S. R., and E. Pottier. 1996. "A Review of Target Decomposition Theorems in Radar Polarimetry." *IEEE Transactions on Geoscience and Remote Sensing* 34 (2): 498–518. doi:10.1109/36.485127.

Cloude, S. R., and E. Pottier. 1997. "An Entropy Based Classification Scheme for Land Applications of Polarimetric SAR." *IEEE Transactions on Geoscience and Remote Sensing* 35 (1): 68–78. doi:10.1109/36.551935.

Delgado, O., J. Ruiz, M. Pérez, J. Romero, and E. Ballesteros. 1999. "Effects of Fish Farming on Seagrass (Posidonia Oceanica) in a Mediterranean Bay: Seagrass Decline after Organic Loading Cessation." *Oceanologica Acta* 22 (1): 109–117. doi:10.1016/S0399-1784(99)80037-1.

Ehler, C., and F. Douvere. 2007 "*Visions for a Sea Change. Report of the First International Workshop on Marine Spatial Planning. Intergovernmental Oceanographic Commission and Man and the Biosphere Programme.*" IOC manual and guides no. 46: ICAM Dossier no. 3, Paris: UNES. doi:10.17605/OSF.IO/U7EAN.

FAO. 2016. *The State of World Fisheries and Aquaculture 2016*. Rome: Food and Agriculture Organization of the United Nations.

Forrest, B. M., N. B. Keeley, G. A. Hopkins, S. C. Webb, and D. M. Clement. 2009. "Bivalve Aquaculture in Estuaries: Review and Synthesis of Oyster Cultivation Effects." *Aquaculture* 298 (1–2): 1–15. doi:10.1016/j.aquaculture.2009.09.032.

Freeman, A., and S. L. Durden. 1998. "A Three-Component Scattering Model for Polarimetric SAR Data." *IEEE Transactions on GeoScience and Remote Sensing* 36 (3): 963–973. doi:10.1109/36.673687.

International EMECS Center. 2001. "Enclosed Coastal Seas of Japan [In Japanese]." https://www.emecs.or.jp/encsea/japan

Komatsu, T., T. Sagawa, S. Sawayama, H. Tanoue, A. Mohri, and Y. Sakanishi. 2012. "Mapping Is a Key for Sustainable Development of Coastal Waters: Examples of Seagrass Beds and

Aquaculture Facilities in Japan with Use of ALOS Images." In *Sustainable Development-Education, Business and Management-Architecture and Building Construction-Agriculture and Food Security*, edited by C. Ghenai, 145–160. Rijeka: InTech.

Komatsu, T., M. Takahashi, K. Ishida, T. Suzuki, T. Hiraishi, and H. Tameishi. 2002. "Mapping of Aquaculture Facilities in Yamada Bay in Sanriku Coast, Japan, by IKONOS Satellite Imagery." *Fisheries Science* 68 (sup1): 584–587. doi:10.2331/fishsci.68.sup1_584.

Ottinger, M., K. Clauss, and C. Kuenzer. 2016. "Aquaculture: Relevance, Distribution, Impacts and Spatial Assessments – A Review." *Ocean & Coastal Management* 119: 244–266. doi:10.1016/j.ocecoaman.2015.10.015.

Shimada, M., N. Kawano, M. Watanabe, T. Motooka, and M. Ohki 2013. "Calibration and Validation of the Pi-SAR-L2." *Synthetic Aperture Radar (APSAR), 2013 Asia-Pacific Conference on*: 194–197. IEEE. doi:10.1177/1753193413475963.

Sugimoto, M., K. Ouchi, and Y. Nakamura. 2013. "Comprehensive Contrast Comparison of Laver Cultivation Area Extraction Using Parameters Derived from Polarimetric Synthetic Aperture Radar Data." *Journal of Applied Remote Sensing* 7 (1): 073566. doi:10.1117/1.JRS.7.073566.

Szuster, B. W., C. Steckler, and B. Kullavanijaya. 2008. "Detecting and Managing Coastal Fisheries and Aquaculture Gear Using Satellite Radar Imagery." *Coastal Management* 36 (3): 318–329. doi:10.1080/08920750801968330.

Travaglia, C., G. Profeti, J. Aguilar-Manjarrez, and N. A. Lopez 2004. "*Mapping Coastal Aquaculture and Fisheries Structures by Satellite Imaging Radar: Case Study of the Lingayen Gulf, the Philippines*." FAO Fisheries Technical paper No 459. Rome: Food and Agriculture Organization of the United Nations.

Tsujimoto, R., G. Terauchi, H. Sasaki, S. X. Sakamoto, S. Sawayama, S. Sasa, H. Yagi, and T. Komatsu. 2016. "Damage to Seagrass and Seaweed Beds in Matsushima Bay, Japan, Caused by the Huge Tsunami of the Great East Japan Earthquake on 11 March 2011." *International Journal of Remote Sensing* 37 (24): 5843–5863. doi:10.1080/01431161.2016.1249300.

UNCED, F. 1992, "*Agenda 21*." The United Nations Programme of Action from Rio, 3. New York, NY: United Nations Department of Public Information.

Van Zyl, J. J. 1989. "Unsupervised Classification of Scattering Behaviour Using Radar Polarimetry Data." *IEEE Transactions on Geoscience and Remote Sensing* 27: 36–45. doi:10.1109/36.20273.

Won, E. S., K. Ouchi, and C. S. Yang. 2013. "Extraction of Underwater Laver Cultivation Nets by SAR Polarimetric Entropy." *IEEE Geoscience and Remote Sensing Letters* 10 (2): 231–235. doi:10.1109/LGRS.2012.2199077.

World Bank. 2013. "*Fish to 2030 Prospects for Fisheries and Aquaculture*." World Bank Report, No. 83177- GLB. Washington, DC: World Bank.

Yamaguchi, Y., T. Moriyama, M. Ishido, and H. Yamada. 2005. "Four-Component Scattering Model for Polarimetric SAR Image Decomposition." *IEEE Transactions on Geoscience and Remote Sensing* 43 (8): 1699–1706. doi:10.1109/TGRS.2005.852084.